ACS APPLIED MATERIALS & INTERFACES
Research Article
www.acsami.org

Creating Graphene p–n Junctions Using Self-Assembled Monolayers

Hossein Sojoudi,[†] Jose Baltazar,[‡] Laren M. Tolbert,[‡] Clifford L. Henderson,[‡] and Samuel Graham*[,†]

[†]Woodruff School of Mechanical Engineering and School of Materials Science and Engineering, Georgia Institute of Technology, Atlanta, Georgia 30332, United States

[‡]School of Chemistry and Biochemistry, Georgia Institute of Technology, Atlanta, Georgia 30332, United States

ABSTRACT: 3-Aminopropyltriethoxysilane (APTES) and perfluorooctyltriethoxysilane (PFES) were used to modify the interface between transferred CVD graphene films and its supporting dielectric to create n-type and p-type graphene, respectively. A graphene p–n junction was obtained by patterning both modifiers on the same dielectric and verified through the creation of a field effect transistor (FET). Characteristic $I-V$ curves indicate the presence of two separate Dirac points which confirms an energy separation of neutrality points within the complementary regions. This method minimizes doping-induced defects and results in thermally stable graphene p–n junctions for temperatures up to 200 °C.

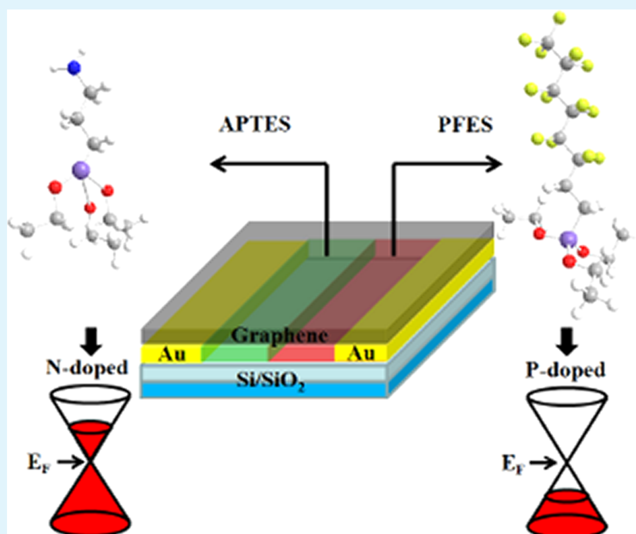

KEYWORDS: *graphene, p–n junction, self-assembled monolayers (SAMs), interface modification, thermally stable doping*

INTRODUCTION

Graphene has exhibited some unique properties that have made it of interest to the scientific community for use as an electronic material. These properties include an unusual band structure that makes it a gapless semiconductor, linear energy-momentum relationship near the Dirac point, and extraordinarily high carrier mobilities.[1−3] Because of the zero-gap in single-layer graphene, both carrier type and concentration can be controlled through an electrostatic gate, making graphene a promising material for semiconductor applications.[2,4] This electrostatic gating allows the development of graphene-based bipolar devices where a junction between hole-rich and electron-rich regions, or a p–n junction, can be formed.[5,6] Graphene p–n junctions have already displayed new and exciting phenomena such as Klein tunneling, where electrons traveling perpendicular to the junction experience zero resistance[7] and fractional quantum Hall transport.[6] Such junctions are predicted to produce lensing effects for coherent electrons, so-called Veselago lensing, where diverging electron waves are refocused by the junction.[8] Most graphene junctions to date have been fabricated using multiple electrostatic gates,[6] electrical stress-induced doping,[9,10] chemical treatment by gas exposure,[11] chemical modifications on top of the graphene,[12−14] and modification of the substrate by changing the local electrostatic potential in the vicinity of one of the contacts.[15] However, current methods for electrostatic gating require a number of fabrication steps that may not be easily scalable in industry level and are usually expensive. Furthermore, chemical doping on top of graphene can degrade the carrier mobility in the device through the introduction of defects and impurities in the graphene. In addition, physisorbed dopant molecules are not stable and may desorb resulting in changes in the electronic properties of the graphene.

Here, we utilize a low temperature controllable method to fabricate p–n junctions in graphene by modifying the interface between graphene and its support substrate with self-assembled monolayers (SAMs). SAMs have been extensively used to enhance the mobility of organic thin film transistors and to eliminate the Schottky barrier at the metal semiconductor interface.[16−19] They have been recently used to modify graphene and dielectric interfaces by reducing charged impurity scattering and the effects of environmentally induced doping on graphene,[20,21] and to control charge carrier and concentration to create n- and p-type graphene field effect transistors (FETs).[22−25] Unlike chemical doping, this method uses SAMs that covalently bond to the substrate rather than graphene, resulting in thermally stable doping independent of the dielectric material and thickness.

Received: June 23, 2012
Accepted: August 21, 2012
Published: August 21, 2012

 © 2012 American Chemical Society

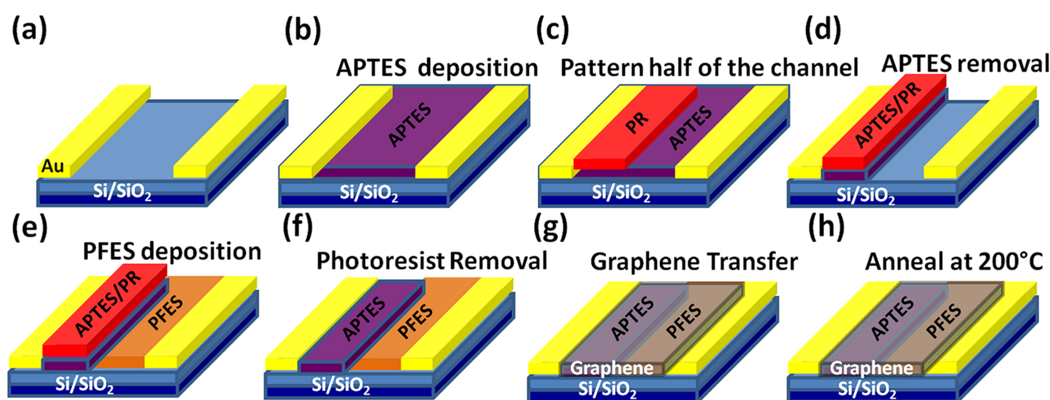

Figure 1. Schematic of the graphene p−n junction fabrication steps.

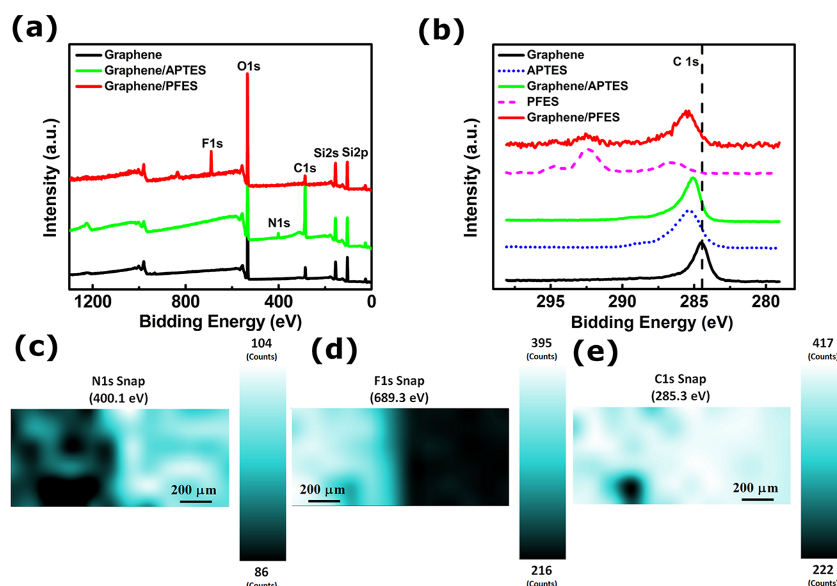

Figure 2. XPS spectra representing (a) survey scan and (b) core level C1s binding energy for graphene/SiO_2 (black), graphene/PFES/SiO_2 (red) and graphene/APTES/SiO_2 (green). XPS mapping of a graphene p−n junction. (c) N1s binding energy centered at 400.1 eV, (d) F1s binding energy centered at 689.3 eV, and (e) C1s binding energy centered at 285.3 eV.

3-Aminopropyltriethoxysilane (APTES) and 1H,1H,2H,2H-Perfluorooctyltriethoxysilane (PFES) were used to modify the interface between transferred layers of CVD graphene and its supporting dielectric to create n- and p- type graphene, respectively. APTES contains an amine functional group with a basic nitrogen atom having a lone electron pair. The electron-rich amine group donates an electron to the carbon atoms in graphene, causing n-doping. In contrast, fluorine is a well-known electron acceptor. Thus, adding a layer of PFES results in the transfer of an electron from the graphene creating p-type graphene. The purpose of the silane group is to create a strong covalent bond to the oxide dielectric support such as SiO_2, thereby anchoring the APTES and PFES which induces thermal stability of the modified interface and the doped graphene layer. By patterning adjacent regions of APTES and PFES, p−n junctions in the graphene were created.

EXPERIMENTAL SECTION

The fabrication process of the graphene p−n junction is schematically illustrated in Figure 1. First, the source and drain contacts (gold 50 nm thick) were defined using conventional photolithography and lift-off processes on a highly p-doped Si substrate with a 300 nm thick SiO_2 layer to create back gated field effect transistor structures. The resulted channel size was 25 μm × 25 μm. Prior to APTES deposition, the substrate was first pretreated by UV ozone for 15 min in order to produce a hydroxyl-terminated substrate that reacts with the silane coupling agent. Immediately afterward, the substrate was immersed in a 0.1%(v/v) solution of anhydrous toluene and 3-aminopropyltrietoxysilane (APTES) for 3 h, producing a free-amine-rich substrate with a contact angle of ~60°. Next, half of the channel in the FET device was patterned with photoresist. After exposure and development, the other half of the channel was treated with UV-Ozone for 15 min to remove the exposed APTES and produce a hydroxyl-terminated surface. Next, the device was treated for one hour with 100 μL of PFES dissolved in 10 mL of toluene 1%(v/v). The measured contact angle for PFES-treated substrate was ca. 110°. Finally, the resist was removed to expose the APTES coated region prior to transfer of graphene on top of the SAMs coated SiO_2. Monolayer graphene was grown on a 25 μm thick sheet of Cu foil (Alfa Aesar, item No. 14482) in a low pressure environment using chemical vapor deposition (CVD) and transferred to the device through a similar method explained in the literature.[8]

RESULTS AND DISCUSSION

Characteristics of Functionalized Device. X-ray photoelectron spectroscopy was employed to identify the surface functionalization present on the SiO_2 on each side of the channel to confirm the presence of APTES and PFES. XPS data

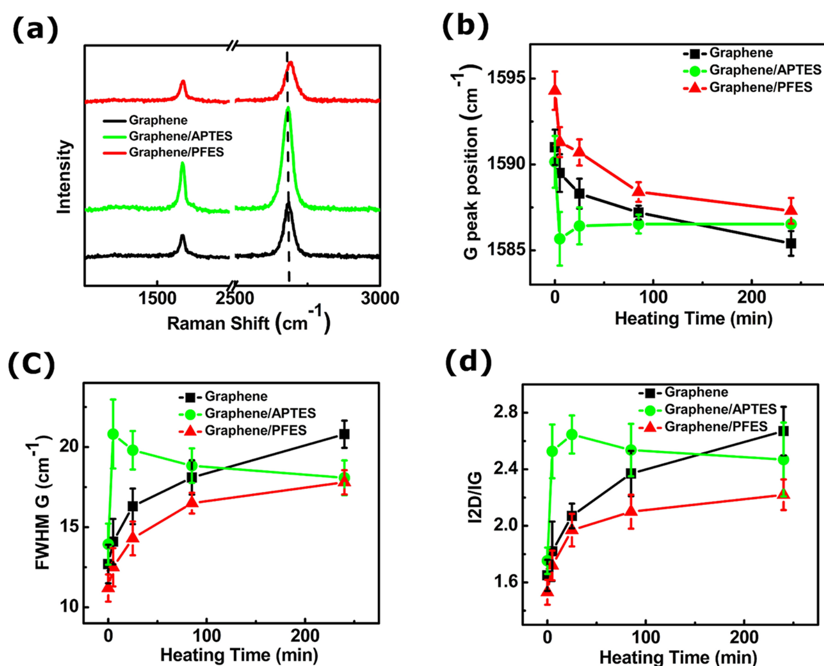

Figure 3. (a) Raman spectra of graphene/SiO_2(black), grapheen/APTES/SiO_2 (green), and graphene/PFES/SiO_2 (red) after being heated at 200 °C under nitrogen atmosphere for 3 h. (b–d) G peaks position, FWHM (G), and I_{2D}/I_G as a function of heating time under nitrogen atmosphere for graphene/SiO_2, graphene/APTES/SiO_2, and graphene/PFES/SiO_2.

were acquired using a spectrophotometer (VG Scientific ESCALAB 210) with an Kα X-ray source ($h\nu$ = 1486.68 eV). The survey scan spectra were collected at the binding energy (B.E.) of 0–1300 eV with a step size of 1 eV at a pass energy of 200 eV and a spot size of 400 μm. Figure 2a shows survey scan spectra randomly collected from as-transferred graphene, functionalized with APTES, and with PFES. The scan showed the most prominent peaks to be C1s and O1s on all spectra. The appearance of a N1s peak centered at 400.1 eV and a F1s peak centered at 689.3 eV in the survey spectra confirms the presence of APTES and PFES underneath the graphene, respectively. High resolution XPS spectra of the C1s binding energy was also acquired over 282–293 eV with a step size of 0.1 and 50 eV pass energy. The appearance of a shoulder and a shift in the C1s peak position of functionalized graphene also verified the presence of APTES and PFES on the substrate (see Figure 2b). To ensure the presence and formation of the patterned SAMs on the channel, XPS mapping was utilized (see Figure 2c–e). XPS mapping was performed using a 30 μm spot size with a step size of 28 μm, and a Gaussian smoothing algorithm was applied to the raw data. Figure 2c shows the intensity of the N1s map with a well-defined boundary that indicates the presence of amine only on half of the channel. Similarly, the F1s map indicates the presence of fluorine in the other half of the channel (see Figure 2d). For the core level C1s mapping, a binding energy centered at 285.3 eV was selected.

In Situ Raman Spectroscopy. It is well-known that environmentally induced water vapor and oxygen bound to the graphene are electron acceptors[26] that play an important role in the unintentional p-doping of graphene films.[27] This unintentional doping had to be removed in order to fully reveal the effects of the APTES and PFES on the graphene. To remove this unintentional doping effect, we heat-treated the samples under nitrogen atmosphere to unmask the intentional doping effects of the APTES and the PFES underlying layer.[28] To this end, the samples were cycled between room temperature and 200 °C from 5 to 180 min while in situ Raman spectroscopy was utilized at room temperature to investigate the quality of the graphene and its doping state by examining the D, G, and 2D bands and their positions. All spectra were excited with visible (532 nm) laser light and collected in the backscattering configuration. The samples were placed inside an environmentally controlled microscope stage with heating, vacuum, and gas delivery capability (Linkam TS 1500) for in situ Raman measurements. Raman measurements were performed before and after annealing under nitrogen. Figure 3a shows the Raman spectra of as-transferred, APTES treated, and PFES treated graphene after 3 h of annealing at 200 °C. The difference in the G and 2D peak width, position, and their intensity ratio for each sample is indicative of various doping states. A critical observation is that no increase on the D band was observed during any of the annealing steps; hence successful doping of the graphene monolayer without significant damage to the lattice structure was achieved.[29,30] Monitoring of the G peak position with increase in heating time, its full width at half-maximum FWHM (G), and intensity ratio of 2D over G peak (I_{2D}/I_G) reveal the changes in electronic state of various devices. Figure 3b shows a decrease in the G peak position of as-transferred graphene after annealing for only 5 min. Further annealing resulted in a greater decrease in the peak position, leading to 1588 cm^{-1} after 3 h of annealing. This indicates the dedoping process induced by the removal of the environmentally induced dopants through annealing.[27,31] Panels c and d in Figure 3 show an increase in FWHM (G) from 17 to 23 and I_{2D}/I_G from 1.685 to 1.7, respectively. These confirm the removal of atmospheric p-dopant, leading to dedoped graphene after 3 h of heat treatment. The G peak position of as-transferred graphene functionalized with APTES was 1590 cm^{-1} with FWHM (G) at 14 cm^{-1}. These are lower than the values for graphene without functionalization with APTES and are indicative of a reduction in p-doping state. This change in the G peak position is due to competing effects between n-

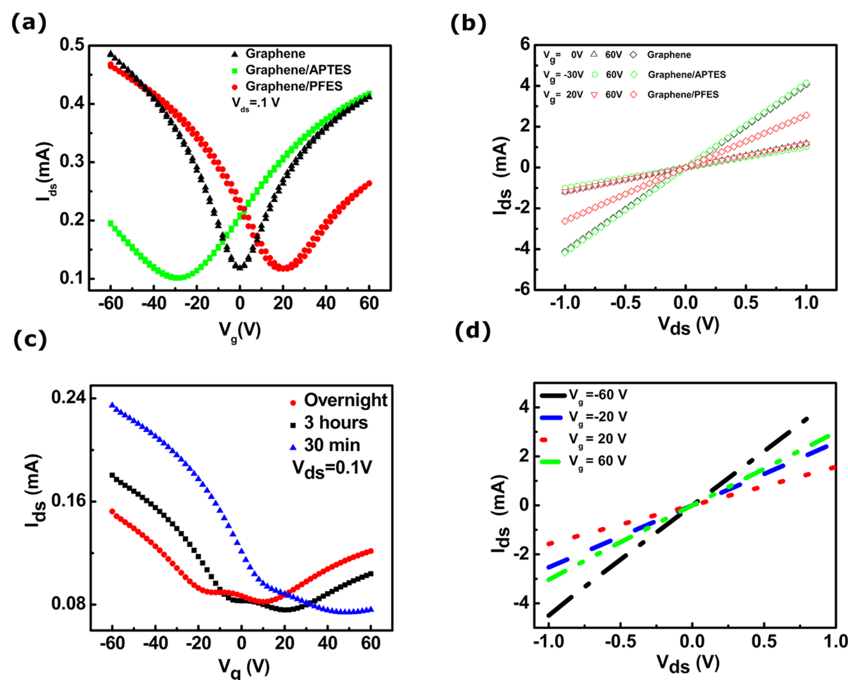

Figure 4. (a) Drain-source current versus gate voltage for graphene/SiO_2 (black), graphene/APTES/SiO_2 (green) and graphene/PFES/SiO_2(red) after being heated at 200 °C for 3 h under nitrogen environment. (b) I_{ds}−V_{ds} characteristic of the graphene, graphene/APTES, and graphene/PFES devices at different gate voltages. (c) Drain-source current versus gate voltage as a function of heating time for a graphene p−n junction. (d) I_{ds}−V_{ds} characteristic of the graphene p−n junction at different gate voltages.

doping induced by APTES and p-doping by water vapor and oxygen.[27] Similar to as-transferred graphene, heat treatment for 5 min resulted in the removal of p-dopants, leading to a decrease in G peak position down to 1585.5 cm^{-1}, an increase in FWHM (G) to 21 and I_{2D}/I_G to 2.65. These values are similar to those measured for dedoped graphene. However, further heat treatment resulted in the removal of additional p-dopants, causing the n-doping effect to become dominant. This led to an increase in the G peak position to 1586.5 cm^{-1} and a decrease in FWHM (G) to 20 and I_{2D}/I_G to 2.3, which is in accord with observed Raman characteristics for n-doped graphene.[33]

The trend in Raman characteristics for PFES functionalized graphene is similar to that obtained with as-transferred graphene. A heavily p-doped characteristic before heat treatment is due to the presence of both PFES and atmospheric dopants from water vapor and oxygen.[27] However, removal of atmospheric dopants by heat treatment for 3 h results in lowering the p-doping level in the graphene with a 7 cm^{-1} decrease in the G peak position, 6 cm^{-1} increase in FWHM (G), and 0.7 increase in I_{2D}/I_G. The shift in the position of the G peak is indicative of induced doping by SAMs without a change in the structure of graphene.

Electrical Data Measurements. To further demonstrate the n-type and p-type characteristics induced by APTES and PFES in graphene, back-gated FET devices were fabricated as shown in Figure 1. Here, the difference is that the devices were only treated with APTES or PFES. Another set of devices were fabricated without SAMs as control devices. Transport in the APTES- and PFES-treated graphene devices as well as the devices without SAMs was measured using a probe station equipped with a HP 4156 semiconductor parameter analyzer under a nitrogen atmosphere (see Figure 4a). It is noteworthy that these measurements were performed after heat treatment of the devices up to 200 °C in a nitrogen atmosphere to remove dominant p-dopants resulting from air exposure and the graphene transfer process in order to unmask the intentional doping effect induced by SAMs. The charge neutrality point for graphene without SAMs was around zero volts after 3 h of heat treatment, indicative of dedoped graphene as shown in Figure 4a. It is important to note that further annealing for up to 7 days did not cause a change in the neutrality point in graphene control devices. This is in contrast with the observed n-type characteristic of graphene due to annealing in a nitrogen atmosphere as we saw no evidence of n-type doping in these samples.[12] For the APTES treated device, n-doping characteristics were observed with the charge neutrality point (CNP) stably forming at ca. −30 V after 3 h of heat treatment at 200 °C. For PFES treated device, p-type behavior was observed with charge neutrality point stabilizing at ca. 20 V after 3 h of annealing at the same environment. Drain-source current values, I_{ds}, in the devices with the same channel size did not experience a significant change after being treated with APTES or PFES (see Figure 4a for representative I_{ds}−V_g curves). Several APTES and PFES-treated devices were fabricated and similar results were obtained for each set of devices. Figure 4b demonstrates the I_{ds}−V_{ds} output characterization for graphene, graphene/APTES, and graphene/PFES at variable back-gate voltages (V_g). The linear I_{ds}−V_{ds} behavior in all devices indicates the lack of a significant Schottky barriers and good ohmic contact at the Au-graphene interface. For graphene devices without SAMs, at any given value for V_{ds}, I_{ds} is minimum for V_g = 0 V, indicative of dedoped graphene. This change in the I_{ds} value at any given values for V_{ds} was observed at V_g = 20 V and V_g = −30 V for graphene/PFES and graphene/APTES indicative of p- and n-doping, respectively. Unlike the sample without SAMs, intentional doping by APTES and PFES was shown to be thermally stable, as there

was no change in the neutrality point after removal of the atmospheric dopants via thermal annealing in nitrogen. The electron and hole concentration of the APTES and PFES-treated graphene after annealing was approximately 1.92 ± 0.1 × 10^{12} cm^{-2} and 1.53 ± 0.07 × 10^{12} cm^{-2}, respectively. These values were calculated using the equation, $n = C_g V_{np}/e$,[32,33] where C_g = 115 aF/μm^2,[34] e is the charge of the electron and V_{np} is the voltage at the charge neutrality point. Electron and hole field-effect mobilities for graphene/APTES devices were 6210 ± 890 cm^2/(V s) and 4761 ± 609 cm^2/(V s), respectively. These values for graphene/PFES were 6443 ± 350 cm^2/(V s) and 4326 ± 171 cm^2/(V s) for hole and electron mobilities, respectively. The electron and hole mobilities for graphene devices without SAMs are 4560 ± 678 cm^2/(V s) and 5212 ± 805 cm^2/(V s) which are of the same order of magnitude with APTES/PFES-treated devices. These values are extracted using the relation $\mu_{FE} = L_{ch} g_m / W_{ch} V_{ds} C_{ox}$,[34] where L_{ch} = 25 μm, g_m = dI_{ds}/dV_g (peak value), W_{ch} = 25 μm, V_{ds} = 0.1 V, and C_{ox} = 115 aF/μm^2,[34] indicating that the SAMs have only a minor effect, if any, on the mobility of graphene devices.[23,35] Typically, an increase in the charge carrier concentration via doping can result in a decrease in the mobility due to intrinsic scattering of the carriers. In addition, the slight difference in the mobility and the minimum current of APTES and PFES-treated devices can be due to the differences in the transferred graphene that has origins in varying grain size or transfer process of CVD graphene.

Electrical data measurements were performed on fabricated p−n junctions in a nitrogen atmosphere using a method similar to that explained earlier (see Figure 4c). As-fabricated devices indicated p-type characteristics due to excess amount of atmospheric dopants. After annealing at 200 °C a shift in the charge neutrality point to lower values was observed that indicates removal of atmospheric dopants. This annealing controls the position of the junction in the I_{ds}−V_g curve until the neutrality point for the p- side of the channel is reached. When the annealing time increased to 3 h, two Dirac points (peaks) were seen in the I_{ds}−V_g curve: one located at $V_{np} \approx 20$ V and the other at $V_{np} \approx -5$ V. Annealing overnight resulted in a sharp p−n junction behavior with two neutrality points located at V_{np} = 10 V and V_{np} = −18 V, which indicates an energy separation of the neutrality points within the complementary regions. A drain voltage sweeping from V_{ds} = −1 V to V_{ds} = 1 V was performed and I_{ds} was plotted for various V_g values (see Figure 4d). For a given V_{ds}, an increase in V_g from 20 to 60 V results in an increase in I_{ds} indicative of p-type characteristic, and a decrease in V_g from 20 to −20 V causes an increase in I_{ds} demonstrating n-type characteristic in a single p−n junction device. Unlike conventional semiconductor p−n junction, I_{ds}−V_{ds} curves do not show rectifying behavior. This is due to the chirality of the massless Dirac fermions of graphene that results in suppression of backscattering by potential barriers (Klein tunneling).[7] The amount of free amines and fluorine available on the substrate can be tuned by varying the APTES and PFES deposition time to fully control the transport behavior of the fabricated p−n junction.

SUMMARY

In summary, we utilized APTES and PFES to induce n- and p-type characteristics in graphene without altering its structure. These SAMs bond to the substrate and are thermally stable. Simultaneous use of these groups in a FET device results in formation of two separate Dirac points, as indicative of a graphene p−n junction. Variation in the duration of substrate functionalizing with these SAMs and heat treatment period results in p−n junctions with controlled position and height.

AUTHOR INFORMATION

Corresponding Author

*E-mail: sgraham@gatech.edu.

Author Contributions

H.S. and J.B. contributed equally.

Notes

The authors declare no competing financial interest.

ACKNOWLEDGMENTS

This material is based upon work supported by the National Science Foundation under Grants CHE-0822697, CHE-0848833, and CMMI-0927736 and the Georgia Tech MRSEC.

REFERENCES

(1) Du, X.; Skachko, I.; Barker, A.; Andrei, E. Y. *Nat. Nanotechnol.* **2008**, *3*, 491−495.
(2) Novoselov, K. S.; Geim, A. K.; Morozov, S. V.; Jiang, D.; Zhang, Y.; Dubonos, S. V.; Grigorieva, I. V.; Firsov, A. A. *Science* **2004**, *306*, 666−669.
(3) Novoselov, K. S.; Geim, A. K.; Morozov, S. V.; Jiang, D.; Katsnelson, M. I.; Grigorieva, I. V.; Dubonos, S. V.; Firsov, A. A. *Nature* **2005**, *438*, 197−200.
(4) Ohta, T.; Bostwick, A.; Seyller, T.; Horn, K.; Rotenberg, E. *Science* **2006**, *313*, 951−954.
(5) Abanin, D. A.; Levitov, L. S. *Science* **2007**, *317*, 641−643.
(6) Williams, J. R.; DiCarlo, L.; Marcus, C. M. *Science* **2007**, *317*, 638−641.
(7) Katsnelson, M. I.; Novoselov, K. S.; Geim, A. K. *Nat. Phys.* **2006**, *2*, 620−625.
(8) Cheianov, V. V.; Fal'ko, V.; Altshuler, B. L. *Science* **2007**, *315*, 1252−1255.
(9) Yu, T. H.; Liang, C. W.; Kim, C. D.; Yu, B. *Appl. Phys. Lett.* **2011**, *98*, 243105.
(10) Rao, G.; Freitag, M.; Chiu, H. Y.; Sundaram, R. S.; Avouris, P. *ACS Nano* **2011**, *5*, 5848−5854.
(11) Lohmann, T.; von Klitzing, K.; Smet, J. H. *Nano Lett.* **2009**, *9*, 1973−1979.
(12) Brenner, K.; Murali, R. *Appl. Phys. Lett.* **2010**, *96*, 063104.
(13) Peters, E. C.; Lee, E. J. H.; Burghard, M.; Kern, K. *Appl. Phys. Lett.* **2010**, *97*, 193102.
(14) Farmer, D. B.; Lin, Y.-M.; Afzali-Ardakani, A.; Avouris, P. *Appl. Phys. Lett.* **2009**, *94*, 213106.
(15) Chiu, H.-Y.; Perebeinos, V.; Lin, Y.-M.; Avouris, P. *Nano Lett.* **2010**, *10*, 4634−4639.
(16) Kobayashi, S.; Nishikawa, T.; Takenobu, T.; Mori, S.; Shimoda, T.; Mitani, T.; Shimotani, H.; Yoshimoto, N.; Ogawa, S.; Iwasa, Y. *Nat. Mater.* **2004**, *3*, 317−322.
(17) Ito, Y.; Virkar, A. A.; Mannsfeld, S.; Oh, J. H.; Toney, M.; Locklin, J.; Bao, Z. A. *J. Am. Chem. Soc.* **2009**, *131*, 9396−9404.
(18) Pernstich, K. P.; Haas, S.; Oberhoff, D.; Goldmann, C.; Gundlach, D. J.; Batlogg, B.; Rashid, A. N.; Schitter, G. *J. Appl. Phys.* **2004**, *96*, 6431−6438.
(19) Vosgueritchian, M.; LeMieux, M. C.; Dodge, D.; Bao, Z. N. *ACS Nano* **2010**, *4*, 6137−6145.
(20) Liu, Z. H.; Bol, A. A.; Haensch, W. *Nano Lett.* **2011**, *11*, 523−528.
(21) Park, J.; Lee, W. H.; Huh, S.; Sim, S. H.; Kim, S. B.; Cho, K.; Hong, B. H.; Kim, K. S. *J. Phys. Chem. Lett.* **2011**, *2*, 841−845.
(22) Wang, R.; Wang, S.; Zhang, D.; Li, Z.; Fang, Y.; Qiu, X. *ACS Nano* **2011**, *5*, 408−412.
(23) Yan, Z.; Sun, Z. Z.; Lu, W.; Yao, J.; Zhu, Y.; Tour, J. M. *ACS Nano* **2011**, *5*, 1535−1540.

(24) Shin, W. C.; Seo, S.; Cho, B. J. *Appl. Phys. Lett.* **2011**, *98*, 153505.
(25) Wang, X. M.; Xu, J. B.; Wang, C. L.; Du, J.; Xie, W. G. *Adv. Mater.* **2011**, *23*, 2464−2468.
(26) Schedin, F.; Geim, A. K.; Morozov, S. V.; Hill, E. W.; Blake, P.; Katsnelson, M. I.; Novoselov, K. S. *Nat. Mater.* **2007**, *6*, 652−655.
(27) Sojoudi, H.; Baltazar, J.; Henderson, C.; Graham, S. *J. Vac. Sci Technol. B* **2012**, *30*, 041213.
(28) Ni, Z. H.; Wang, H. M.; Luo, Z. Q.; Wang, Y. Y.; Yu, T.; Wu, Y. H.; Shen, Z. X. *J. Raman Spectrosc.* **2010**, *41*, 479−483.
(29) Yokota, K.; Takai, K.; Enoki, T. *Nano Lett.* **2011**, *11*, 3669−3675.
(30) Das, A.; Pisana, S.; Chakraborty, B.; Piscanec, S.; Saha, S. K.; Waghmare, U. V.; Novoselov, K. S.; Krishnamurthy, H. R.; Geim, A. K.; Ferrari, A. C.; et al. *Nat. Nanotechnol.* **2008**, *3*, 210−215.
(31) Shen, Z. X.; Ni, Z. H.; Wang, H. M.; Luo, Z. Q.; Wang, Y. Y.; Yu, T.; Wu, Y. H. *J. Raman Spectrosc.* **2010**, *41*, 479−483.
(32) Nourbakhsh, A.; Cantoro, M.; Klekachev, A.; Clemente, F.; Soree, B.; van der Veen, M. H.; Vosch, T.; Stesmans, A.; Sels, B.; De Gendt, S. *J. Phys. Chem. C* **2010**, *114*, 6894−6900.
(33) Joselevich, E.; Tsivion, D.; Schvartzman, M.; Popovitz-Biro, R.; Von Huth, P. *Science* **2011**, *333*, 1003−1007.
(34) Schwierz, F. *Nat. Nanotechnol.* **2010**, *5*, 487−496.
(35) Wang, R.; Wang, S.; Zhang, D.; Li, Z.; Fang, Y.; Qiu, X. *ACS Nano* **2010**, *5*, 408−412.